

Re-examining Temporal Variations in Intermediate-Depth Seismicity

Sam Wimpenny^{1,*}, Tim Craig¹, and Savvas Marcou^{1,2}

¹COMET, Institute for Geophysics and Tectonics,
School of Earth and Environment, University of Leeds, UK.

²Now at: Berkeley Seismological Laboratory, University of California, Berkeley,
Berkeley, California, U.S.A.

Emails: **earswi@leeds.ac.uk*

1 Abstract

2 Changes in the frequency of intermediate-depth (60–300 km) earthquakes in response to static stress
3 transfer can provide insights into the mechanisms of earthquake generation within subducting slabs.
4 In this study, we use the most up-to-date global and regional earthquake catalogues to show that
5 both aftershock productivity, and the changes in the frequency of intermediate-depth earthquakes
6 around the timing of major megathrust slip, support the view that faults within the slab are relatively
7 insensitive to static stress transfer on the order of earthquake stress drops. We interpret these results to
8 suggest the population of faults within the slab are much further from their failure stress than is typical
9 for shallow faults, and that the mechanism that enables faults to rupture at the high confining pressures
10 within slabs is likely to be spatially heterogeneous over length-scales of a few tens of kilometres. We
11 suggest dehydration-related weakening mechanisms can best account for this heterogeneity.

12
13 *This paper is a pre-print, therefore has not finished peer review and is currently being considered for*
14 *publication in Journal of Geophysical Research – Solid Earth.*

15 **Plain Language Summary**

16 Earthquakes at 60–300 km depth within subducting slabs are known as ‘intermediate-depth’ earth-
17 quakes. At such depths, the high pressures should act to clamp faults shut, preventing them from
18 breaking in earthquakes through frictional sliding. In this study, we investigate the mechanisms
19 that enable the generation of intermediate-depth earthquakes by examining the temporal changes of
20 intermediate-depth seismicity caused by other, nearby earthquakes. We find that seismicity within
21 slabs is relatively insensitive to static stress transfer caused by nearby earthquakes. We interpret these
22 results to suggest that faults within the slab are much further from their failure stress than is typical
23 for shallow faults, and that the mechanism that enables faults to rupture at intermediate depth is
24 likely to be spatially variable over length-scales of a few tens of kilometres. We suggest weakening
25 mechanisms related to water release within slabs can best account for this heterogeneity.

26 **Key Points:**

- 27 • Large intraslab and megathrust earthquakes have a limited influence the frequency of
28 intermediate-depth seismicity.
- 29 • Faults within subducted slabs are relatively insensitive to static stress transfer caused by earth-
30 quake stress drops.
- 31 • Low stress drops and heterogeneous aftershock productivity can be best explained by
32 dehydration-related weakening mechanisms.

33 1 Introduction

34 Temporal variations in the frequency of intermediate-depth (60–300 km) seismicity have the potential
35 to provide insights into the enigmatic conditions and mechanism(s) of earthquake nucleation within
36 subducting slabs. Intraslab earthquakes have dominantly double-couple focal mechanisms, indicating
37 they represent shear failure on a population of faults [Frohlich, 1989]. However, at depths $\gtrsim 60$ km, the
38 high confining pressures and temperatures should prevent frictional failure on faults subject to normal
39 plate-driving forces without an additional rheological mechanism that reduces the stress needed to
40 generate earthquake rupture [Zhan, 2020].

41 Two main mechanisms have been proposed: dehydration-related weakening and self-localising thermal
42 runaway. Dehydration-related weakening is caused by the breakdown of hydrous mafic minerals as
43 the slab subducts, which either releases water that reduces the effective frictional strength of intraslab
44 faults (dehydration embrittlement; Green and Houston [1995]; Hacker et al. [2003]), or causes extreme
45 stress concentrations through the breakdown of load-bearing hydrous phases (dehydration-assisted
46 stress transfer; Ferrand et al. [2017]), allowing faults to fail through frictional sliding. Alternatively,
47 self-localising thermal runaway is a process by which creep in hydrated or fine-grained shear zones
48 causes shear heating and the development of ductile instabilities that relax elastic strain [Ogawa, 1987;
49 Hobbs and Ord, 1988]. Thermal runaway may have a nucleation phase involving progressive ductile
50 strain, eventually leading up to seismogenic failure that relaxes the majority of the stored elastic
51 strain in high stress-drop events (500–1000 MPa; Kelemen and Hirth [2007]; John et al. [2009]). These
52 different mechanisms can account for earthquake generation at high confining pressures, but they are
53 sensitive to different physical and mechanical conditions within the slab, such as temperature and the
54 availability of hydrous mineral phases.

55 Progress in our understanding of intermediate-depth earthquake generation has mainly focused on
56 explaining the spatial pattern of seismicity within subduction zones, such as the structure of double-
57 seismic zones [e.g. Wei et al., 2017; Florez and Prieto, 2019; Sippl et al., 2019], or the relationship
58 between intermediate-depth earthquake focal mechanisms, seismicity rates, and the orientation and
59 density of outer-rise normal faulting [e.g. Warren et al., 2007; Boneh et al., 2019]. Analysis of any
60 temporal variations in the frequency of intermediate-depth seismicity can potentially provide com-
61 plimentary information to these studies. In particular, variations in the frequency of seismicity in
62 response to known stress changes can provide insights into the population of faults that are close to
63 failure, as well as the sensitivity of the failure mechanism to small stress perturbations, and how these

64 vary between different pressure-temperature conditions and slab environments [e.g. Tibi et al., 2003;
65 Persh and Houston, 2004; Zhan and Shearer, 2015; Bouchon et al., 2016, 2018; Luo and Wiens, 2020].

66 Two observations have emerged that suggest different sensitivities of intraslab faults systems to changes
67 in static stress. First, studies have reported changes in the frequency of intraslab intermediate-depth
68 earthquakes related to the occurrence of shallow earthquakes, including: (1) year-long changes in
69 earthquake frequency that begin after large, shallow earthquakes on the adjacent subduction megathrust
70 [Lay et al., 1989; Bouchon et al., 2016; Jara et al., 2017; Mitsui et al., 2021], and (2) month-long
71 transient changes in intraslab earthquake frequency following slip on the megathrust [Delbridge et al.,
72 2017]. These observations suggest that intraslab faults in some settings are relatively sensitive to the
73 small ($\ll 1$ MPa) stress changes that shallow earthquakes impose on the slab through static stress
74 transfer, and that faults within the subduction system are interacting with one another over distances
75 of tens to hundreds of kilometres. In contrast, intermediate-depth earthquakes are often followed by
76 low productivity aftershock sequences compared to shallow crustal earthquakes of similar magnitude
77 [Frohlich, 1987; Wiens and Gilbert, 1996; Persh and Houston, 2004; Ye et al., 2020]. As the stress
78 drops in intermediate-depth earthquakes are similar to shallow earthquakes (~ 1 – 50 MPa) [Allmann
79 and Shearer, 2009; Poli and Prieto, 2016; Tian et al., 2022], the difference in aftershock productiv-
80 ity between shallow and intermediate-depth mainshocks is not related to the amplitude of the stress
81 changes. Rather, the deficiency of intermediate-depth aftershock sequences indicates that the faults
82 within the slab are relatively insensitive to the stress changes caused by nearby large earthquakes
83 within the slab, and that they only weakly interact with one another. These two inferences relating
84 to intraslab seismicity are in clear contradiction. This study aims to reconcile them.

85 We re-examine the changes in intermediate-depth earthquake frequency around the timing of large
86 earthquakes using the most up-to-date global and regional earthquake catalogues. Section 2 focuses on
87 the aftershock sequences of intermediate-depth earthquakes, verifying previous results regarding their
88 aftershock-deficient nature. Section 3 then explores the response of intermediate-depth seismicity to
89 slip in megathrust earthquakes. We find that, although there are temporal variations in the frequency
90 of intermediate-depth seismicity, they do not consistently correlate with the stress changes caused
91 by large megathrust earthquakes. In Section 4, we discuss the implications of our findings for the
92 mechanics of faulting at intermediate depths within slabs.

93 2 Aftershock Productivity of Intermediate-Depth Earthquakes

94 Aftershocks are the most obvious manifestation of changes in seismicity rates, and reflect the rupture
95 of fault patches in response to stress changes from a larger earthquake [King et al., 1994]. Aftershock
96 sequences following intermediate-depth earthquakes typically contain fewer events (less ‘productive’)
97 compared to shallow earthquakes of equivalent magnitude [Frohlich, 1987; Wiens and Gilbert, 1996;
98 Dascher-Cousineau et al., 2020]. Aftershock productivity is also known to be depth-dependent, with
99 most large earthquakes between 300–500 km often having no aftershocks at all with $m_b \geq 4.5$ [Persh
100 and Houston, 2004]. Early studies suggested that productivity correlates with a slab’s thermal struc-
101 ture [Wiens and Gilbert, 1996], though more recent work using longer-duration catalogues with lower
102 magnitudes of completeness has argued that productivity is independent of slab temperature, but may
103 be related to the heterogeneity of the stress field and fault network surrounding the mainshock [Ye
104 et al., 2020] or fluid conditions in the slab [Cabrera et al., 2021; Chu and Beroza, 2022].

105 Below, we re-examine aftershock productivity at both global and regional scales using modern earth-
106 quake catalogues, focusing particularly on seismicity within the depth range 60–300 km. Through
107 this updated analysis, we aim to characterise the relative sensitivity of intraslab fault systems to
108 earthquake stress changes in different settings.

109 2.1 Global Analysis

110 We first studied the aftershock sequences of $M_w > 6.5$ earthquakes using a simple clustering algorithm
111 applied to hypocentral location and origin time estimates in the ISC’s reviewed global catalogue fol-
112 lowing the method of Baiesi and Paczuski [2004] and Zaliapin et al. [2008]. We use this non-parametric
113 clustering method, as it does not assume any particular form for the temporal evolution of aftershock
114 frequency. The ISC’s reviewed earthquake catalogue is derived from a location procedure that uses
115 the body-wave phase arrivals from teleseismic and regional stations to provide the most accurate esti-
116 mates of earthquake hypocentral parameters and consistent body-wave magnitude estimates globally
117 [Bondár and Storchak, 2011; Di Giacomo and Storchak, 2016]. We complement these data with the
118 earthquake moment tensor information for each mainshock derived using long-period body and surface
119 wave inversion from the global Centroid Moment Tensor (gCMT) catalogue [Dziewonski et al., 1981;
120 Ekström et al., 2012]. The time-span of our analysis is limited to between 1976 and 2020.

121 For each mainshock, we began by subsetting the ISC catalogue to events that are within 500 km of the

122 mainshock hypocentre and which have $m_b \geq 4.5$. For all events within this subset, we then calculated
 123 the space-time distance η_{ij} between each event hypocentre i and every other event hypocentre j
 124 [Zaliapin et al., 2008]. The space-time distance is defined as $\eta_{ij} = t_{ij}(r_{ij})^d 10^{-bm_i}$, where $t_{ij} = t_j - t_i$ is
 125 the time difference between event origin times, r_{ij} is the 3-dimensional cartesian distance between the
 126 event hypocentres, m_i is the magnitude of event i , and $d = 1.6$ and $b = 1$ are constants [Zaliapin and
 127 Ben-Zion, 2013]. If $t_{ij} \leq 0$ then we set $\eta_{ij} = \infty$ to enforce causality (i.e. event j must have occurred
 128 after event i for it to be an aftershock). The choice of $m_b \geq 4.5$ is designed to capture a global average
 129 for the magnitude of completeness for intermediate-depth seismicity [Ye et al., 2020], though changing
 130 this value to $m_b \geq 5.0$ has little affect on the trends in productivity (Supplementary Text S1).

131 For every event j in the catalogue we define its parent as the event i for which $\eta_j = \min(\eta_{ij})$. At
 132 this stage we check that the mainshock is not an aftershock of an even larger earthquake by ensuring
 133 that, for the event to be considered a mainshock, it has no parent events that have magnitude a
 134 larger magnitude. The resulting distribution of $\log_{10}(\eta_j)$ forms two peaks (Supplementary Figure 1a),
 135 with events with low $\log_{10}(\eta_j)$ being clustered events and those with high $\log_{10}(\eta_j)$ being independent
 136 events [Zaliapin et al., 2008; Zaliapin and Ben-Zion, 2013]. To determine the cut-off between the
 137 two, we fit a two-component Gaussian mixture model to the distribution and determined the overlap
 138 between the two curves η_0 (Supplementary Figure 1b). We then recursively counted all of the off-
 139 spring of the mainshock that have $\eta_j \leq \eta_0$ to yield the final aftershock count [Zaliapin and Ben-Zion,
 140 2013]. The seismicity that is not clustered (i.e. all events for which $\eta_j > \eta_0$) is used to calculate
 141 the background seismicity rate within ± 50 km horizontal distance and ± 30 km depth around each
 142 mainshock (Supplementary Figure 2). This analysis yields aftershock counts for 2432 mainshocks. For
 143 the remaining 1586 events with $M_w \geq 6.5$ in the gCMT catalogue, we were either not able to separate
 144 the background from the clustered seismicity, or the earthquake was itself an aftershock. Although the
 145 absolute aftershock count is weakly dependent on the constants used in the space-time distance calcu-
 146 lation (b , d , and η_0), the relative count between mainshocks is insensitive to the parameter selection
 147 [Zaliapin and Ben-Zion, 2013] (Supplementary Text S1).

148 Our analysis shows that the median aftershock productivity decreases significantly at 50–60 km depth
 149 (Figure 1a), which roughly corresponds to the transition from shallow crustal and intraplate seismicity
 150 to only intraslab seismicity. Below 60 km depth, the median productivity decreases with depth until
 151 300 km, remains consistently low for mainshocks between 300 km and 500 km depth, and then increases
 152 between 500 km and 700 km depth, mirroring the distribution of mainshocks (Figure 1a).

153 For earthquakes within the intermediate-depth range (60–300 km), the maximum and median produc-

154 tivity increases with mainshock magnitude as $a10^{b(M-m_c)}$ where $b \approx 1$ [Frohlich, 1987], but remains
155 consistently lower than for shallow earthquakes (Figure 1b). There is no correlation between the
156 productivity and the date of the mainshock, suggesting temporal changes in the ISC catalogue's com-
157 pleteness is not masking any trends (Figure 1c). The productivity does not correlate with the gradient
158 in down-dip slab curvature or background seismicity rate (Figure 1d,e), which implies that aliasing
159 high rates of background seismicity into aftershock productivity is also not biasing the results. We also
160 find that the productivity does not vary depending on whether the mainshock mechanism is accom-
161 modating along-strike deformation or down-dip deformation of the slab (Figure 1f). Irrespective of
162 the relationship between the mechanism of the mainshock and the slab geometry, 70% of mainshocks
163 have no recorded aftershocks with $m_b \geq 4.5$ (Figure 1f). Only 40% of earthquakes with hypocentral
164 depths < 50 km have no aftershocks. These conclusions also hold after removing the scaling between
165 mainshock magnitude and the median aftershock productivity (Supplementary Figure 5).

166 Based on this analysis, we confirm the observations derived from older catalogues that mainshock
167 depth and magnitude correlate with the aftershock productivity [Frohlich, 1987; Persh and Houston,
168 2004; Ye et al., 2020]. Our analysis highlights for the first time the significant decrease in productivity
169 between shallow earthquakes and intermediate-depth earthquakes, and the slight depth-dependence of
170 productivity for intermediate-depth earthquakes (Supplementary Text S2). However, some physical
171 process(es) must be controlling the observed *range* in aftershock productivity between intraslab events
172 of similar magnitude [Frohlich, 1987]. One possibility is that these process(es) relate to the mechanical
173 properties of the slab [e.g. Wiens and Gilbert, 1996], or the stress heterogeneity within the slab [e.g.
174 Ye et al., 2020], in which case productivity would vary spatially within and between subduction
175 zones. We did not find any systematic spatial variability in aftershock productivity at the scale of
176 individual subduction zones. For example, large earthquakes beneath South America typically have
177 low productivity compared to the global average [Ye et al., 2020], though the productive aftershock
178 sequence of the M_w 7.9 2005 Tarapaca earthquake beneath northern Chile is a clear exception to this
179 trend (Supplementary Text S2). However, most regions have too few $M_w \geq 7.5$ events to identify
180 any robust trends, and smaller earthquakes in the magnitude range $6.5 \leq M_w < 7.5$ have too few
181 aftershocks (i.e. < 10) of $m_b \geq 4.5$ to record spatial variability in the productivity (Supplementary
182 Text S2). Therefore, stress heterogeneity and features unique to a particular slab, at least at the scale
183 of hundreds of kilometres, seem unable to explain our measured differences in aftershock productivity,
184 but more large earthquakes are required to robustly test these hypotheses using global catalogue data.

185 2.2 Regional Analysis: Northern Chile

186 High-resolution regional earthquake catalogues can provide better constraints on the spatial variability
187 in aftershock productivity and its relationships with the mainshock setting [Sippl et al., 2019; Gomberg
188 and Bodin, 2021; Chu and Beroza, 2022]. We re-assessed the aftershock productivity of moderate-
189 magnitude earthquakes in northern Chile, because this region has: (1) an earthquake catalogue that
190 contains over 100,000 earthquakes of $M_L \geq 2.0$ from between 2006 and 2015 [Sippl et al., 2018], (2) a
191 highly seismogenic slab at intermediate depths, and (3) relatively consistent earthquake mechanisms
192 and magnitudes that allows for comparison between events with a similar source.

193 We applied the same aftershock identification algorithm to the catalogue of Sippl et al. [2018] for
194 all moderate-magnitude earthquakes with $M_w \geq 5.3$ and include all events above the completeness
195 $M_L \geq 2.8$ [Sippl et al., 2018] as possible aftershocks (Figure 2). This leads to aftershock counts for 114
196 earthquakes. In this small study region, where almost all of the intermediate-depth earthquakes ac-
197 commodate down-dip extension of the slab (Figure 2a), we find that maximum productivity increases
198 with the mainshock magnitude and decreases with depth [see also Sippl et al., 2019], but there is vari-
199 ability in productivity that cannot be explained by these parameters alone (Figure 2b-d). Earthquakes
200 that have near-identical magnitudes, focal mechanisms, hypocentral depths, and which are in similar
201 parts of the slab, can have significant differences in the number of aftershocks they produce (Figure
202 2b,c). Cabrera et al. [2021] suggested that the aftershock productivity may decrease systematically as
203 a function of distance below the slab surface using six well-located mainshocks. We did not find this
204 pattern when considering the a set of 114 mainshocks (Figure 2d). However, more accurate estimates
205 of the mainshock hypocentral depths and the slab surface geometry may update this view.

206 Similar analyses to the one presented above have been performed for intermediate-depth earthquakes
207 in Cascadia [Gomberg and Bodin, 2021] and Japan [Chu and Beroza, 2022]. The analysis from
208 Cascadia included 63 mainshocks and used a catalogue complete down to $M_L = 1.9$. Gomberg and
209 Bodin [2021] also found that the aftershock productivity increased with mainshock magnitude and
210 decreased with mainshock depth, though with significant scatter to the data. A notable difference
211 between Cascadia and northern Chile is that the background seismicity rate correlates weakly with the
212 aftershock productivity in Cascadia, whilst we did not find this trend in either our global analysis or for
213 northern Chile (Supplementary Text S3). The analysis of aftershock productivity in Japan included 64
214 mainshocks and used the JMA catalogue, which is complete to $M_{JMA} = 2.0$. Chu and Beroza [2022]
215 found that the productivity of intermediate-depth earthquakes was consistently lower than shallow

216 earthquakes of equivalent magnitude, and that productivity increased with magnitude. However, there
217 was not enough variability amongst the intermediate-depth events to determine whether productivity
218 varied with depth. Chu and Beroza [2022] found that around half of all events have no recorded
219 aftershocks, whilst for those that do have aftershock sequences the productivity scales with the V_p/V_s
220 ratio in the region. In northern Chile, we find more of a continuum of aftershock productivity, but
221 our results support the view of Chu and Beroza [2022] that something in addition to just depth and
222 magnitude must be influencing the variability in aftershock productivity.

223 In summary, the deficiency of intermediate-depth aftershock sequences suggests the faults within
224 subducting oceanic lithosphere are less likely to rupture in response to an earthquake stress drop
225 compared to shallow faults. All studies consistently observe an increase in productivity with mainshock
226 magnitude as 10^{bM_w} , which is likely a result of larger mainshocks having larger rupture areas A with
227 $A \propto 10^{M_w}$ causing stress changes on a larger fault area, or in a larger volume, surrounding the
228 mainshock rupture [Wetzler et al., 2016]. The slight decrease in the productivity with depth suggests
229 that the number of faults able to rupture in response to a mainshock decreases as depth increases,
230 which indicates a depth-sensitive failure or weakening mechanism. Although there are clear differences
231 in aftershock productivity between intraslab earthquakes of similar magnitude, we did not find any
232 robust evidence that suggests the relative sensitivity of fault systems varies systematically between
233 different slab settings. Rather, productivity seems to be heterogeneous at the scale of individual
234 subduction zones and within individual slabs, suggesting the mechanism that controls productivity is
235 also heterogeneous over length-scales of tens of kilometres. In the next section, we explore whether
236 intraslab faults are also insensitive to slip on the subduction interface in major megathrust earthquakes.

237 **3 Response of Intermediate-Depth Seismicity to Megathrust Slip**

238 **3.1 Global Analysis**

239 Intraslab faults will experience stress changes in response to slip on the megathrust. These stress
240 changes have been suggested to modulate the frequency of earthquakes that accommodate down-dip
241 extension or compression within the slab [Astiz et al., 1988; Dmowska et al., 1988; Lay et al., 1989].
242 To test whether these inferences are robust, we first extended the analysis of Astiz et al. [1988] and
243 Lay et al. [1989] using the modern gCMT catalogue [Dziewonski et al., 1981; Ekström et al., 2012].
244 For every megathrust earthquake between 1990 and 2017 with $M_w \geq 8.0$, we extracted all of the

245 surrounding earthquakes from the gCMT with centroid depths in the range 60–300 km and that are
246 within ± 200 km of the projection of the megathrust earthquake’s T -axis in the down-dip direction of
247 the slab. We then removed all earthquakes with centroids that are above the slab surface defined by
248 Slab 2.0 [Hayes et al., 2018]. We also repeated the analysis but without excluding events based on
249 their position relative to the slab, given that both the slab surface and the earthquake centroid depths
250 can be uncertain by ± 10 km or more, but found this had only a minor effect on the resulting patterns.

251 Astiz et al. [1988] suggested that down-dip compressional earthquakes at intermediate depths are
252 more frequent after megathrust earthquakes, and down-dip extensional earthquakes less frequent, as
253 megathrust slip causes incremental down-dip compression of the slab. Therefore, to assign each earth-
254 quake to either down-dip compression or extension, we filtered the events based on the angle between
255 their P , T , and N -axes and the normal and dip vector of the slab derived from Slab 2.0. Earthquakes
256 are associated with down-dip compression if the T -axis is within 45° of the slab normal, the N -axis
257 makes an angle greater than 45° with the slab normal, and the P -axis makes an angle greater than
258 45° with the slab dip vector. The same filter was used to isolate down-dip extensional earthquakes,
259 but with the constraint that the P -axis is within 45° of the slab normal vector. Earthquakes that do
260 not fit these two conditions (denoted ‘other’ in the analysis below) mostly accommodate along-strike
261 deformation of the slab or shearing of the slab in the plane parallel to the slab dip direction (slab
262 tearing). We also assess the temporal variability in these events to ensure that the method of data
263 selection does not bias the results.

264 To examine changes in the frequency of intermediate-depth earthquakes associated with megathrust
265 slip, we calculated the difference in the number of earthquakes before (N_b) and after (N_a) the main-
266 shock at time t_0 . We then divide this by the total number of earthquakes in the period $[t_0 - \Delta t, t_0 + \Delta t]$,
267 yielding a value $\Delta N/N = (N_a - N_b)/(N_a + N_b)$ that is in the range $[-1, 1]$. A value of 1 means all
268 earthquakes of a particular mechanism occurred after the mainshock, whilst -1 means they all oc-
269 curred before the mainshock. We calculated $\Delta N/N$ for all earthquakes with magnitude $M \geq M_c$
270 where M_c is in the range $[5.0, 6.0]$ and for Δt of 5 years or 10 years. This simple approach captures
271 the rate changes without relying on any assumptions about the statistical distribution of seismicity in
272 time, as a more complex approach is not warranted by the limited number of earthquakes.

273 The analyses of three different earthquakes illustrate the key results (Figure 3). For the 2011 M_w
274 9.1 Tohoku-oki earthquake, the largest event in the gCMT catalogue, there are only 12 down-dip
275 extensional and 21 down-dip compressional earthquakes at intermediate depths within 20 years of the
276 mainshock (Figure 3a). All of the down-dip extensional earthquakes with $M_w \geq 5.5$ occurred prior to

277 Tohoku-oki, and there were no down-dip extensional earthquakes in the 10 years following. Evidence
 278 for changes in the frequency of down-dip compressional earthquakes is less clear, as there are too
 279 few events (Figure 3a). Therefore, the extensional seismicity down-dip of the Tohoku-oki mainshock
 280 appears to follow the trend predicted by the model of Astiz et al. [1988]. The slab down-dip of the
 281 2001 M_w 8.1 Arequipa earthquake is far more seismogenic compared to Japan, with predominantly
 282 down-dip extensional seismicity as the slab bends into the mantle beneath the Andes (Figure 3b). The
 283 number of down-dip extensional earthquakes systematically increased following slip on the megathrust
 284 in the Arequipa earthquake, which is opposite to the trend expected if megathrust slip puts the
 285 slab into incremental down-dip compression and inhibits down-dip extensional earthquakes. The
 286 intermediate-depth seismicity down-dip of the 2006 M_w 8.2 Kermadec earthquake shows a different
 287 result again. In this region, the majority of the intermediate-depth earthquakes are associated with
 288 down-dip compression. We find no robust change in the frequency of down-dip extensional earthquakes
 289 caused by megathrust slip. However, the data suggests that the number of down-dip compressional
 290 earthquakes with $M_w \geq 5.5$ decreased after megathrust slip, which is again contrary to the prediction
 291 that megathrust earthquakes promote down-dip compressional seismicity.

292 The three examples in Figure 3 demonstrate that changes in the frequency of earthquake mechanisms
 293 associated with down-dip extension or compression can occur around megathrust earthquakes, but
 294 they are not necessarily consistent between events. To further demonstrate this point, we performed
 295 the following simple test. For every mainshock j , we assign a decrease in rate $\Delta N/N < 0$ a value
 296 of $n_j = -1$ and an increase in rate $\Delta N/N > 0$ a value of $n_j = 1$ for a given time-span Δt relative
 297 to the mainshock and magnitude cut-off M_c . We then compute $\sum_{j=1}^k n_j(M_c, \Delta t)$ for all megathrust
 298 mainshocks $j = \{1, 2, \dots, k\}$. If there is a consistent pattern of rate increases after the mainshock, then
 299 $\sum_{j=1}^k n_j(M_c, \Delta t) > 0$, whilst a rate decrease would be associated with $\sum_{j=1}^k n_j(M_c, \Delta t) < 0$. This
 300 process is equivalent to a 1-dimensional simple random walk. In the case of the null hypothesis that
 301 an increase in seismicity is equally likely as a decrease, the expected value of $\sum_{j=1}^k n_j(M_c, \Delta t)$ is 0
 302 and the standard deviation is \sqrt{k} . The results of this stacking process are shown in Figure 4.

303 For down-dip extensional seismicity the sum $\sum_{j=1}^k n_j(M_c, \Delta t)$ is similar to the expected value for the
 304 null hypothesis (Figure 4a), suggesting there is no consistent change in down-dip extension of the
 305 slab after megathrust earthquakes. Down-dip compressional seismicity does typically increase after
 306 megathrust earthquakes, but only for intermediate-depth earthquakes with $M_w \leq 5.5$ (Figure 4b),
 307 which is around the magnitude of completeness of the gCMT catalogue [Kagan, 2003]. The smallest
 308 M_w 5 earthquakes are also likely to have the largest depth and mechanism uncertainties [Wimpenny

309 and Watson, 2020], and so thrust-faulting on the megathrust may be incorrectly assigned to being
310 within the slab. The amplitude of the deviation from the expected value for the null hypothesis
311 for earthquakes $M_w > 5.5$ is smaller than 2 standard deviations, therefore we cannot reject the
312 hypothesis that these changes in earthquake frequency are random when only considering events
313 above the magnitude of completeness. Given that down-dip extension, compression, and other types
314 of earthquake mechanisms at intermediate-depths generally increase in frequency in the 5–10 years
315 after a mainshock (Figure 4a-c), and the increase becomes more robust for longer time-spans Δt , then
316 these trends most likely reflect the increase in the gCMT catalogue completeness through time.

317 In summary, we find no robust evidence in the gCMT catalogue for systematic changes in the frequency
318 of moderate-to-large magnitude earthquakes accommodate down-dip deformation of the slab in the
319 intermediate-depth range. In the next two sections, we test whether the apparent lack of triggered
320 intraslab seismicity might reflect the limited number of earthquakes within the gCMT catalogue by
321 focusing on two regions with extensive intraslab seismicity and high-quality regional catalogues.

322 **3.2 Regional Analysis: Japan**

323 Japan has the highest-resolution earthquake catalogue of any subduction zone due to the dense onshore
324 seismic network, and is therefore an ideal natural laboratory for this type of analysis. Delbridge et al.
325 [2017] previously reported an increase in intermediate-depth seismicity down-dip of the rupture area of
326 the 2011 Tohoku-oki earthquake in the upper plane of the double-seismic zone (DSZ) recorded by the
327 regional earthquake catalogue, which consists mostly of compressional earthquakes accommodating
328 unbending of the Pacific plate. Our analysis of the earthquake moment tensors from the gCMT
329 catalogue failed to identify such a trend (Figure 3a). We therefore re-analysed the frequency variations
330 of intermediate-depth earthquakes recorded in the JMA catalogue down-dip of the Tohoku-oki rupture
331 area (Figure 5a,b). A total of 6595 intermediate-depth earthquakes occurred in this region between
332 2006 and 2019 that are >100 km from the trench and >60 km deep, and which are larger than the
333 magnitude of completeness of the catalogue ($M_{JMA} = 2.0$). We assigned events to the upper or lower
334 plane of the DSZ by binning the event depths relative to Slab 2.0 as a function of distance from the
335 trench and fitting a Gaussian mixture model to the relative depth distributions.

336 From this analysis, we confirm there is a spike in the frequency of earthquakes assigned to the upper
337 plane within a month of the Tohoku-oki mainshock, with the rate increasing from ~ 0.5 earthquakes
338 per day to nearly 6 per day (Figure 5c). There is no clear change in the frequency of lower-plane

339 earthquakes over the same period. The peak seismicity rate in the upper plane occurred 1 month after
340 the mainshock and decayed over 7 years before returning to the background rate in 2018. However, this
341 result is extremely sensitive to the cut-off depth (Figure 5d). For an identical analysis of earthquakes
342 that have depths >70 km, the spike in earthquake frequency disappears and there is no clear deviation
343 from the pre-Tohoku seismicity (Figure 5e). The large number of earthquakes in the JMA catalogue
344 allows us to test the statistical significance of the seismicity rate changes using the β -statistic of
345 Matthews and Reasenbergl [1988], which shows that there are no variations in the earthquake frequency
346 for events >70 km that are greater than 2 standard deviations from the pre-Tohoku seismicity (Figure
347 5f). An analysis of the seismicity in the ISC reviewed catalogue from the same region, which support
348 our observations made using the JMA catalogue, is discussed in Supplementary Text S4.

349 Further investigation revealed that the seismicity contributing to the spike in earthquake frequency
350 in the upper plane in Figure 5c mostly derived from the region of the 7th April 2011 M_w 7.2 Miyagi-
351 oki reverse-faulting earthquake, which ruptured the slab at ~ 55 – 65 km depth less than a month
352 after the Tohoku-oki mainshock. Removing the seismicity within 50 km of the Miyagi-oki earthquake
353 suppresses the spike in the intermediate-depth seismicity rate (Supplementary Text S4). It is also
354 possible that the ~ 5 – 10 km uncertainties in earthquake hypocentral depths for small earthquakes in
355 the JMA catalogue mean that some aftershocks occurring at the down-dip edge of the megathrust, or
356 within the overriding plate, are mislocated and have been incorrectly assigned to the upper plane of
357 the DSZ [e.g. Sippl et al., 2019]. To test this possibility, we removed all events that are within 10 km
358 of the plate interface from the analysis, which also suppresses the spike in seismicity rate related to
359 the Tohoku-oki and Miyagi-oki earthquakes (Supplementary Text S4). Therefore, we conclude that
360 the change in earthquake frequency identified by Delbridge et al. [2017] may not indicate a slab-wide
361 increase in intermediate-depth earthquake frequency in response to the 2011 Tohoku-oki earthquake,
362 but rather the aftershock sequence of the Miyagi-oki earthquake (Figure 5b, inset). This difference
363 is important, because it suggests that the majority of faults that are definitively within the slab are
364 insensitive to the stress changes caused by megathrust slip in the Tohoku-oki earthquake.

365 **3.3 Regional Analysis: Northern Chile**

366 Megathrust slip has also been proposed to modulate intermediate-depth seismicity in northern Chile.
367 Jara et al. [2017] suggested that the 1995 Antofagasta and 2014 Iquique megathrust earthquakes
368 were followed by periods of reduced moderate-magnitude seismicity at intermediate depths beneath
369 northern Chile, whilst the 2005 Tarapaca intraslab earthquake was followed by nine years of increased

370 seismicity at both shallow and intermediate depths (Figure 6a,b). Since Jara et al. [2017]’s original
371 analysis, Sippl et al. [2018] has published an earthquake catalogue spanning 2006–2015 in northern
372 Chile that is complete down to $M_L = 2.8$, which allows us to examine the changes in intermediate-
373 depth earthquake frequency before and after the Iquique earthquake in more detail. We calculated the
374 earthquake rate through time using the moving window analysis described in Section 3.2, but found
375 no significant deviations in the frequency of intermediate-depth seismicity following the 2014 Iquique
376 earthquake or the 2007 Tocopilla earthquake (Figure 6c,d).

377 The catalogue of Sippl et al. [2018] is too short to capture any of the multi-year trends in earthquake
378 frequency identified by Jara et al. [2017]. Therefore, we re-analysed the temporal variations in seis-
379 micity in northern Chile between 1980 and 2020 using four more years of data in the ISC’s reviewed
380 catalogue than were available to Jara et al. [2017] (Figure 6a). An important limitation in comparing
381 temporal variations in the shallow and intermediate-depth seismicity in this region is that the ISC
382 catalogue’s magnitude of completeness is higher for shallow earthquakes that are offshore ($m_b = 4.7$)
383 than for intermediate-depth earthquakes that are beneath the land ($m_b = 4.3$; see Supplementary Text
384 S5). To ensure that this spatial variability in completeness does not bias our analysis, we only studied
385 events with $m_b \geq 4.7$, which for the region shown on Figure 6 includes 925 earthquakes between
386 1980 and 2020. The annual variations in the frequency of shallow (<50 km) and intermediate-depth
387 (70–170 km) earthquakes are shown as histograms in Figure 6e-f, and as a cumulative distribution
388 in Figure 7a. The depth intervals were selected to closely replicate the analysis of Jara et al. [2017].
389 Unlike Jara et al. [2017], however, we describe the trends in the undeclustered catalogue, and present
390 the equivalent analyses of the declustered catalogue in the Supplementary Information. We take this
391 approach, because the deficiency of intermediate-depth aftershock sequences means that declustering
392 has little effect on the trends in intermediate-depth earthquake frequency through time.

393 There is little shallow seismicity in northern Chile between 1980 and 2007 with typically fewer than 5
394 earthquakes per year with $m_b \geq 4.7$ (Figure 6e), which makes identifying any changes in earthquake
395 frequency during this period difficult. There are so few events in 1980–2007 that the cumulative
396 earthquake distribution with time is not significantly different (<2 standard deviations) from synthetic
397 catalogues that contain the same number of events but with randomised times (Figure 7b), suggesting
398 the shallow seismicity contains no robust information about temporal changes in earthquake frequency
399 in response to the 1995 Antofagasta, 2001 Arequipa, or 2005 Tarapaca earthquakes. Between the 2007
400 Tocopilla and 2014 Iquique earthquakes the annual number of shallow earthquakes increased (Figure
401 6e), which is associated with the well-documented foreshock sequence of the Iquique earthquake [Ruiz

402 et al., 2014]. The Iquique earthquake is then followed by an extensive aftershock sequence that lasts
403 until the end of the catalogue in 2020 (Figures 6e and 7a).

404 At intermediate depths the seismicity is more frequent and variable through time (Figure 6f). Between
405 1980 and 1995 the annual earthquake frequency changes from year-to-year (Figure 6f), but does not
406 deviate from the behaviour of time-randomised catalogues (Figure 7c). During 1980–1995, pulses
407 of seismicity occurred in 1983, 1985, and 1990 that were not associated with a large megathrust or
408 intermediate-depth earthquake (Figure 7c, black arrows). After 1995, there are two distinct changes
409 in the earthquake frequency that last for multiple years: first a decrease around the timing of the 1995
410 Antofagasta earthquake and then an increase around the timing of the 2001 Arequipa earthquake
411 (Figure 6f). This period of seismic quiescence at intermediate-depths between 1995 and 2001 appears
412 to be robust in northern Chile for magnitudes at least 0.5 units larger than the catalogue completeness
413 (Figure 6f). After 2001, we found no evidence for robust changes in the intermediate-depth earthquake
414 frequency caused by the 1987 Antofagasta, 2007 Tocopilla, and 2014 Iquique earthquakes (Figure 7c,d).

415 Our observations support the view that temporal changes in intermediate-depth earthquake frequency
416 in northern Chile did occur, and in some cases lasted for multiple years. However, they are not
417 consistently associated with megathrust earthquakes or large intermediate-depth earthquakes. If there
418 were a consistent physical reason for the frequency changes in response to megathrust slip, then
419 it is unclear why they should occur for only two megathrust events out of six between 1980 and
420 2020. In addition, using the longer earthquake catalogue, we found that the 2014 Iquique megathrust
421 earthquake had no resolvable effect on the frequency of intermediate-depth earthquakes within the
422 slab directly down-dip from the rupture area. Therefore, we argue that large megathrust earthquakes
423 are not the cause of changes in earthquake frequency at intermediate depths beneath northern Chile.

424 **4 Discussion**

425 **4.1 Stress Sensitivity of Intermediate-Depth Seismicity**

426 We initially set out to reconcile two contrasting views of intermediate-depth seismicity: one that
427 suggested intraslab fault systems are sensitive to small stress changes associated with megathrust
428 earthquakes, and another that suggested intraslab fault systems are insensitive to the stress changes
429 caused by large intraslab earthquakes. Our analyses support the view that intermediate-depth seis-
430 micity within subducting slabs is relatively insensitive to static stress transfer as a result of slip in

431 large earthquakes with typical stress drops ($\sim 1\text{--}50$ MPa; see Allmann and Shearer [2009]; Poli and
432 Prieto [2016]; Tian et al. [2022]). This insensitivity is manifest as consistently low aftershock pro-
433 ductivity of intermediate-depth earthquakes, and no consistent triggering of down-dip compressional
434 seismicity, or inhibition of down-dip extensional seismicity, within slabs following megathrust slip. We
435 also did not find any clear evidence that the sensitivity of intraslab faults to static stress transfer
436 varies systematically between subduction zones.

437 The lack of seismicity triggered by static stress transfer at intermediate depths is in stark contrast to
438 the extensive seismicity that is triggered within the outer rise and outer trench-slope region following
439 many major megathrust earthquakes that slip to the trench [Christensen and Ruff, 1983; Bilek and Lay,
440 2018]. The triggered outer-rise seismicity is in similar host material to intermediate-depth seismicity,
441 just at shallower depths, lower confining pressures, and lower temperatures. Therefore, the difference
442 in sensitivity to stress change between outer-rise and intermediate-depth seismicity suggest that either
443 the fault systems in the subducted oceanic lithosphere are not as close to failure as those at the outer
444 rise, or that the mechanism of earthquake generation at intermediate depth is not as sensitive to
445 changes in static stress on the order of earthquake stress drops. This new view of the sensitivity of
446 fault systems within subducted oceanic lithosphere places constraints on the mechanics of earthquake
447 generation at intermediate depths, and the interplay between the source of stress and the mechanism
448 allowing the release of stress in earthquakes on intraslab faults, which we explore further below.

449 4.2 Fault Mechanics of Intermediate-Depth Seismicity

450 Based on the earthquake catalogue data, and recent work on the source properties of intermediate-
451 depth earthquakes, any model of intermediate-depth seismicity should account for three observations:

- 452 1. Intermediate-depth earthquake stress drops (for both mainshocks and aftershocks) should be of
453 a similar order of magnitude to those at shallow depth [Allmann and Shearer, 2009; Poli and
454 Prieto, 2016; Tian et al., 2022].
- 455 2. The response of intermediate-depth seismicity to stress changes on the order of stress drops
456 must be limited, in order to explain the observations of low aftershock productivity and the low
457 sensitivity of intraslab seismicity to slip on the megathrust interface.
- 458 3. There must be *some* capacity to generate limited aftershocks after intermediate-depth earth-
459 quakes, and this capacity should broadly scale with mainshock depth and mainshock magnitude.

460 For shallow faulting, the clock-advance model has proven a simple way of interpreting the sensitivity
461 of fault systems to static stress transfer [King et al., 1994; Hainzl et al., 2010]. In this model after-
462 shocks reflect earthquakes on faults that would have eventually ruptured in response to slow stress
463 accumulation, but occurred earlier than expected due to an additional source of stress. A stress drop
464 of $\Delta\tau$ due to slip in an earthquake leads to stress transfer onto the surrounding faults of magnitude
465 $\mathbf{a}_j\Delta\tau$, where \mathbf{a}_j denotes a vector containing the elastic constants, distance, and relative geometry of
466 the newly stressed fault [Hainzl et al., 2010]. If the faults surrounding the mainshock have a stress
467 distribution τ_j , then any fault patches around the mainshock where $\tau_j + \mathbf{a}_j\Delta\tau > \tau_y$ will rupture in
468 an aftershock (Figure 8a). In Figure 8a we assume that τ_j follows a distribution that is symmetrical
469 about the mean stress, and has a mean value set by the requirement for equilibrium. We also assume
470 that τ_y is roughly constant. Under these assumptions, fewer aftershocks would be produced if the
471 static stress transfer from the mainshock $\mathbf{a}_j\Delta\tau$ is a smaller fraction of the failure stress τ_y , or if the
472 shape of the fault stress population becomes more skewed towards lower stresses. More aftershocks will
473 be produced for larger magnitude earthquakes, because the volume of material around the mainshock
474 that experiences stress changes will be larger meaning the curve in Figure 8a will be taller.

475 A simple prediction of the clock-advance model is that for a given background seismicity rate r and
476 stressing rate $\dot{\tau}$, then a change in static stress $\Delta\tau$ should lead to a change in the number of earthquakes
477 in a region proportional to $r\Delta\tau/\dot{\tau}$. Our analysis suggests that aftershock productivity for intermediate-
478 depth earthquakes does not correlate with the background seismicity rate within the slab (see also
479 Sippl et al. [2019]; Chu and Beroza [2022]). Similarly, the aftershock productivity does not correlate
480 with the down-dip gradient in slab curvature, which is a proxy for the bending-related loading rate of
481 faults within the slab [Sandiford et al., 2020]. In addition, areas where intermediate-depth seismicity
482 is particularly common (e.g. northern Chile) are not more sensitive to earthquake stress changes
483 than places where the slab has relatively few earthquakes (e.g. central Japan). We suggest these
484 departures from predictions of the clock-advance model may indicate that the stresses sustained by
485 the intraslab fault population are significantly below the failure stress, and changes in the failure stress
486 through fault weakening mechanisms far exceed the stress transfer from earthquake stress drops. The
487 modifications to the clock-advance model for the three main weakening mechanisms proposed to enable
488 intermediate-depth seismicity (dehydration embrittlement, dehydration-assisted stress transfer, self-
489 localising thermal runaway) are shown in Figure 8b-d. We discuss each mechanism, and its ability to
490 account for the three features of intermediate-depth seismicity, in turn below.

491 4.2.1 Dehydration Embrittlement

492 Dehydration embrittlement involves the weakening of fault zones through the build up of highly-
493 pressurised fluids released by the breakdown of hydrous mafic minerals during prograde metamorphism
494 (Figure 8b). For this mechanism, the low stress drops in intermediate-depth earthquakes compared
495 to the stresses required for frictional failure on a fault formed of dry olivine at equivalent depths (~ 1
496 GPa at 100 km depth) may either reflect partial stress release, the low shear stresses needed to break
497 faults with a low effective strength, or some combination of both of these.

498 To simplify the representation of dehydration embrittlement in Figure 8b, we consider two populations
499 of faults within the slab: those that contain highly pressurised fluids, and those that do not. Faults
500 containing pressurised fluid are breaking in earthquakes at a low failure stress (Figure 8b), whilst dry
501 faults will be far from their failure stress because the finite size of the forces acting on the slab can
502 only load them to a fraction of their failure stress. For the dry fault population, static stress transfer
503 is unlikely to trigger aftershocks, because most of the faults support stresses that are a small fraction
504 of the failure stress (Figure 8b, black curve). In contrast, stress transfer could trigger slip on the
505 fault population containing pressurised fluids, with the number of aftershocks being related to the
506 number of faults that have been able to trap and build up high fluid pressures (Figure 8b, blue curve).
507 Pervasive dehydration embrittlement, in which most faults in the slab contain near-lithostatic pore
508 fluids, seems unlikely, as this would cause the intraslab faults to be sensitive to stress transfer, and we
509 would expect an aftershock productivity similar to that seen in the shallow crust or higher.

510 Recent work has highlighted the link between aftershock productivity in the subducted Pacific slab
511 beneath Japan and the V_p/V_s structure of the surrounding medium [Chu and Beroza, 2022], with
512 higher productivity linked to higher V_p/V_s ratios and by inference more fluid, which supports this
513 model. The effects of dehydration embrittlement are expected to be spatially heterogeneous due to its
514 dependence on the availability of hydrous minerals and the trapping of the released fluid in faults, then
515 this mechanism has the capacity to account for the spatial variability in aftershock productivity within
516 slabs. Dehydration embrittlement can therefore account for the observations outlined in Section 4.2.

517 4.2.2 Dehydration-Assisted Stress Transfer

518 An alternative mechanism is dehydration-assisted stress transfer, where the loss of load-bearing capac-
519 ity of hydrous minerals within a mixed-composition aggregate leads to the support of the total force

520 acting on a fault onto a fraction of its surface area, allowing the fault to locally reach its failure stress
521 [Ferrand *et al.*, 2017] (Figure 8c). Whilst the failure stress and stress drops at contact level for this
522 mechanism need to be extremely high (500–1000 MPa), fault-averaged stress drops could be far lower
523 if the fault can rupture through patches of weaker hydrous minerals at low shear stresses to account
524 for the ~ 1 –50 MPa seismologically-observed stress drops. Melting of the rupture plane at high stresses
525 could also lead to a proportion of the stress release being accommodated aseismically as ductile shear-
526 ing during the latter stages of slip, after an initial seismically-radiating phase. The resulting stress
527 transfer onto the surrounding faults would be moderated by elastic parameters, the relative location
528 and fault geometry, plus an additional factor describing the degree to which dehydration-assisted stress
529 transfer concentrates stresses at the contact level ($\mathbf{b}_j \Delta \tau$; Figure 8c).

530 As with dehydration embrittlement, the fault population will support average stresses that are signifi-
531 cantly lower than the failure stress of faults containing dry olivine (Figure 8c, black curve). Following
532 a mainshock the stress transfer onto the surrounding faults will be a small fraction of the total fault
533 strength, but will be boosted by the focusing of the stress onto small asperities described by the factor
534 \mathbf{b}_j . The controls on aftershock productivity will therefore be similar to the dehydration embrittle-
535 ment mechanism described above, as it will depend on the degree to which the surrounding material
536 had already dehydrated, and therefore the proportion of the fault population within the slab that
537 can generate the locally high contact stresses needed for failure (Figure 8c, red curve). Zero or low
538 aftershock productivity will occur where the majority of the weak, hydrous phases have broken down
539 into stronger anhydrous phases, meaning that the factor \mathbf{b}_j is smaller. The relative insensitivity of
540 intermediate-depth seismicity to slip on the subduction interface is a result of the stress transfer being
541 a smaller fraction of the failure stress compared to shallow faulting (Figure 8c). Hence, dehydration
542 stress-transfer can also match the three observational requirements described above.

543 4.2.3 Self-Localising Thermal Runaway

544 The final weakening mechanism is self-localising thermal runaway, in which creep in shear zones causes
545 shear heating and the development of ductile instabilities that relax elastic strain [Ogawa, 1987; Hobbs
546 and Ord, 1988]. Numerical models of self-localising thermal runaway suggest that the stress drops
547 generated by an earthquake are a significant fraction of the fault’s failure stress (often ~ 500 –1000
548 MPa at ~ 1 GPa confining pressure), as the positive feedback between strain and shear heating drives
549 runaway failure that relaxes the majority of the elastic strain stored around the fault [Kelemen and
550 Hirth, 2007; John *et al.*, 2009]. Not all of the stress drop and strain release may be seismogenic, and

551 therefore this mechanism might be consistent with the low seismologically-determined stress drops.
552 However, the resulting stress transfer onto surrounding fault systems $\mathbf{a}_j \Delta \tau$ should be a larger fraction
553 of the failure stress than for the dehydration-based mechanisms described above (Figure 8d).

554 The self-localising thermal runaway weakening mechanism is mostly dependent on the stress state of
555 the given shear zone, and does not require any additional chemical processes to weaken the fault.
556 We would not expect to see sensitivity of intermediate-depth seismicity to the shallow, lower-stress
557 drop megathrust earthquakes because the fault failure stress is much larger than the static stress
558 transfer. However, we might expect aftershock productivity to be similar at intermediate-depths to
559 shallow depths, because the ratio between the amplitude of the static stress transfer $\mathbf{a}_j \Delta \tau$ and the
560 fault failure stress τ_y will be similar to that at shallow depths (Figure 8d). Therefore, self-localising
561 thermal runaway is less consistent with our observations of low intraslab aftershock productivity for
562 intermediate-depth earthquakes.

563 **5 Conclusions**

564 Intermediate-depth earthquakes (60–300 km) produce fewer aftershocks compared to shallow (<60
565 km) earthquakes of similar magnitude. The areas of intermediate-depth seismicity down-dip of major
566 megathrust earthquakes are also insensitive to the static stress transfer on the order of earthquakes
567 stress drops caused by megathrust slip. We interpret the relative insensitivity of intermediate-depth
568 seismicity to static stress transfer to suggest that faults within the slab are further from their fail-
569 ure stress than shallow faults. It follows that the availability of the weakening mechanism is the
570 likely control on intermediate-depth aftershock productivity, and this mechanism is heterogeneous
571 over length-scales of a few tens of kilometres to account for the variability in aftershock productivity
572 within slabs. We suggest dehydration-related weakening mechanisms are most consistent with these
573 observations.

574 **Acknowledgements**

575 The authors were supported in this work by the Royal Society under URF\R1\180088 and
576 RF\ERE\210041. SW and TJC were also supported through COMET, the UK Natural Environ-
577 ment Research Council's Centre for the Observation and Modelling of Earthquakes, Volcanoes, and
578 Tectonics. We also thank Jorge Jara for useful discussions about his work on northern Chile.

579 **Data Availability**

580 All data used in this study are freely available. The ISC catalogue is available from <https://doi.org/10.31905/D808B830>, the gCMT catalogue is available from <https://www.globalcmt.org/>, the
581 JMA catalogue is available from [https://www.data.jma.go.jp/svd/eqev/data/bulletin/index_](https://www.data.jma.go.jp/svd/eqev/data/bulletin/index_e.html)
582 [e.html](https://www.data.jma.go.jp/svd/eqev/data/bulletin/index_e.html), and the IPOC catalogue is available from doi.org/10.5880/GFZ.4.1.2018.001 (all last
583 accessed December 2022). The code used to calculate the aftershock productivity is available from
584 [INSERT ZENODO LINK ON ACCEPTANCE].
585

References

- Allmann, B. P. and Shearer, P. M. (2009). Global variations of stress drop for moderate to large earthquakes. *Journal of Geophysical Research: Solid Earth*, 114(1):B01310.
- Astiz, L., Lay, T., and Kanamori, H. (1988). Large intermediate-depth earthquakes and the subduction process. *Physics of the Earth and Planetary Interiors*, 53(1-2):80–166.
- Baiesi, M. and Paczuski, M. (2004). Scale-free networks of earthquakes and aftershocks. *Physical Review E - Statistical Physics, Plasmas, Fluids, and Related Interdisciplinary Topics*, 69(6):8.
- Bilek, S. L. and Lay, T. (2018). Subduction zone megathrust earthquakes. *Geosphere*, 14(4):1468–1500.
- Bondár, I. and Storchak, D. (2011). Improved location procedures at the International Seismological Centre. *Geophysical Journal International*, 186(3):1220–1244.
- Boneh, Y., Schottenfels, E., Kwong, K., van Zelst, I., Tong, X., Eimer, M., Miller, M. S., Moresi, L., Warren, J. M., Wiens, D. A., Billen, M., Naliboff, J., and Zhan, Z. (2019). Intermediate-Depth Earthquakes Controlled by Incoming Plate Hydration Along Bending-Related Faults. *Geophysical Research Letters*, 46(7):3688–3697.
- Bouchon, M., Marsan, D., Durand, V., Campillo, M., Perfettini, H., Madariaga, R., and Gardonio, B. (2016). Potential slab deformation and plunge prior to the Tohoku, Iquique and Maule earthquakes. *Nature Geoscience*, 9(5):380–383.
- Bouchon, M., Marsan, D., Jara, J., Socquet, A., Campillo, M., and Perfettini, H. (2018). Suspected Deep Interaction and Triggering Between Giant Earthquakes in the Chilean Subduction Zone. *Geophysical Research Letters*, 45(11):5454–5460.
- Cabrera, L., Ruiz, S., Poli, P., Contreras-Reyes, E., Osses, A., and Mancini, R. (2021). Northern Chile intermediate-depth earthquakes controlled by plate hydration. *Geophysical Journal International*, 226(1):78–90.
- Christensen, D. H. and Ruff, L. J. (1983). Outer-rise earthquakes and seismic coupling. *Geophysical Research Letters*, 10(8):697–700.
- Chu, S. X. and Beroza, G. C. (2022). Aftershock productivity of intermediate-depth earthquakes in Japan. *Geophysical Journal International*, 230(1):448–463.
- Dascher-Cousineau, K., Brodsky, E. E., Lay, T., and Goebel, T. H. (2020). What Controls Variations in Aftershock Productivity? *Journal of Geophysical Research: Solid Earth*, 125(2):1–18.

- Delbridge, B. G., Kita, S., Uchida, N., Johnson, C. W., Matsuzawa, T., and Bürgmann, R. (2017). Temporal variation of intermediate-depth earthquakes around the time of the M9.0 Tohoku-oki earthquake. *Geophysical Research Letters*, 44(8):3580–3590.
- Di Giacomo, D. and Storchak, D. A. (2016). A scheme to set preferred magnitudes in the ISC Bulletin. *Journal of Seismology*, 20(2):555–567.
- Dmowska, R., Rice, J. R., Lovison, L. C., and Josell, D. (1988). Stress transfer and seismic phenomena in coupled subduction zones during the earthquake cycle. *Journal of Geophysical Research*, 93(B7):7869–7884.
- Dziewonski, A. M., Chou, T.-A., and Woodhouse, J. H. (1981). Determination of earthquake source parameters from waveform data for studies of global and regional seismicity. *Journal of Geophysical Research: Solid Earth*, 86(B4):2825–2852.
- Ekström, G., Nettles, M., and Dziewoński, A. (2012). The global CMT project 2004–2010: Centroid-moment tensors for 13,017 earthquakes. *Physics of the Earth and Planetary Interiors*, 200:1–9.
- Ferrand, T. P., Hilaret, N., Incel, S., Deldicque, D., Labrousse, L., Gasc, J., Renner, J., Wang, Y., Green, H. W., and Schubnel, A. (2017). Dehydration-driven stress transfer triggers intermediate-depth earthquakes. *Nature Communications*, 8(May):1–11.
- Florez, M. A. and Prieto, G. A. (2019). Controlling Factors of Seismicity and Geometry in Double Seismic Zones. *Geophysical Research Letters*, 46(8):4174–4181.
- Frohlich, C. (1987). Aftershocks and temporal clustering of deep earthquakes. *Journal of Geophysical Research: Solid Earth*, 92(B13):13944–13956.
- Frohlich, C. (1989). The Nature of Deep-Focus Earthquakes. *Annual Review of Earth and Planetary Sciences*, 17(1):227–254.
- Gomberg, J. and Bodin, P. (2021). The Productivity of Cascadia Aftershock Sequences. *Bulletin of the Geological Society of America*, 111(3):1494–1507.
- Green, H. W. and Houston, H. (1995). The mechanics of deep earthquakes. *Annual Review of Earth & Planetary Sciences*, 23(Scholz 1990):169–213.
- Hacker, B. R., Peacock, S. M., Abers, G. A., and Holloway, S. D. (2003). Subduction factory 2. Are intermediate-depth earthquakes in subducting slabs linked to metamorphic dehydration reactions? *Journal of Geophysical Research: Solid Earth*, 108(B1).

- Hainzl, S., Brietzke, G. B., and Zöller, G. (2010). Quantitative earthquake forecasts resulting from static stress triggering. *Journal of Geophysical Research: Solid Earth*, 115(11):1–9.
- Hayes, G. P., Moore, G. L., Portner, D. E., Hearne, M., Flamme, H., Furtney, M., and Smoczyk, G. M. (2018). Slab2, a comprehensive subduction zone geometry model. *Science*, 362(6410):58–61.
- Hobbs, B. E. and Ord, A. (1988). Plastic instabilities: implications for the origin of intermediate and deep focus earthquakes. *Journal of Geophysical Research*, 93(B9):10521–10540.
- Jara, J., Socquet, A., Marsan, D., and Bouchon, M. (2017). Long-Term Interactions Between Intermediate Depth and Shallow Seismicity in North Chile Subduction Zone. *Geophysical Research Letters*, 44(18):9283–9292.
- John, T., Medvedev, S., Rüpke, L. H., Andersen, T. B., Podladchikov, Y. Y., and Austrheim, H. (2009). Generation of intermediate-depth earthquakes by self-localizing thermal runaway. *Nature Geoscience*, 2(2):137–140.
- Kagan, Y. Y. (2003). Accuracy of modern global earthquake catalogs. *Physics of the Earth and Planetary Interiors*, 135(2-3):173–209.
- Kelemen, P. B. and Hirth, G. (2007). A periodic shear-heating mechanism for intermediate-depth earthquakes in the mantle. *Nature*, 446(7137):787–790.
- King, G. C. P., Stein, R. S., and Lin, J. (1994). Static stress changes and the triggering of earthquakes. *Bulletin of the Seismological Society of America*, 84(3):935–953.
- Lay, T., Astiz, L., Kanamori, H., and Christensen, D. H. (1989). Temporal variation of large intraplate earthquakes in coupled subduction zones. *Physics of the Earth and Planetary Interiors*, 54(3-4):258–312.
- Luo, Y. and Wiens, D. A. (2020). High Rates of Deep Earthquake Dynamic Triggering in the Thermal Halos of Subducting Slabs. *Geophysical Research Letters*, 47(8):1–10.
- Matthews, M. V. and Reasenberg, P. A. (1988). Statistical methods for investigating quiescence and other temporal seismicity patterns. *Pure and Applied Geophysics PAGEOPH*, 126(2-4):357–372.
- Mitsui, Y., Muramatsu, H., and Tanaka, Y. (2021). Slow deformation event between large intraslab earthquakes at the Tonga Trench. *Scientific Reports*, 11(1):1–8.
- Ogawa, M. (1987). Shear instability in a viscoelastic material as the cause of deep focus earthquakes. *Journal of Geophysical Research*, 92(B13):13801–13810.

- Persh, S. E. and Houston, H. (2004). Strongly depth-dependent aftershock production in deep earthquakes. *Bulletin of the Seismological Society of America*, 94(5):1808–1816.
- Poli, P. and Prieto, G. A. (2016). Global rupture parameters for deep and intermediate-depth earthquakes. *Journal of Geophysical Research: Solid Earth*, 121(12):8871–8887.
- Ruiz, S., Metois, M., Fuenzalida, A., Ruiz, J., Leyton, F., Grandin, R., Vigny, C., Madariaga, R., and Campos, J. (2014). Intense foreshocks and a slow slip event preceded the 2014 Iquique Mw8.1 earthquake. *Science*, (6201):1165–1169.
- Sandiford, D., Moresi, L. M., Sandiford, M., Farrington, R., and Yang, T. (2020). The Fingerprints of Flexure in Slab Seismicity. *Tectonics*, 39(8).
- Sipl, C., Schurr, B., Asch, G., and Kummerow, J. (2018). Seismicity Structure of the Northern Chile Forearc From $\approx 100,000$ Double-Difference Relocated Hypocenters. *Journal of Geophysical Research: Solid Earth*, 123(5):4063–4087.
- Sipl, C., Schurr, B., John, T., and Hainzl, S. (2019). Filling the gap in a double seismic zone: Intraslab seismicity in Northern Chile. *Lithos*, 346-347:105155.
- Tian, D., Wei, S. S., Wang, W., and Wang, F. (2022). Stress drops of intermediate-depth and deep earthquakes in the Tonga slab. *Journal of Geophysical Research: Solid Earth*.
- Tibi, R., Wiens, D. A., and Inoue, H. (2003). Remote triggering of deep earthquakes in the 2002 Tonga sequences. *Nature*, 424(6951):921–925.
- Warren, L. M., Hughes, A. N., and Silver, P. G. (2007). Earthquake mechanics and deformation in the Tonga-Kermadec subduction zone from fault plane orientations of intermediate- And deep-focus earthquakes. *Journal of Geophysical Research: Solid Earth*, 112(5):1–17.
- Wei, S. S., Wiens, D. A., van Keken, P. E., and Cai, C. (2017). Slab temperature controls on the Tonga double seismic zone and slab mantle dehydration. *Science Advances*, 3(1):1–10.
- Wetzler, N., Brodsky, E. E., and Lay, T. (2016). Regional and stress drop effects on aftershock productivity of large megathrust earthquakes. *Geophysical Research Letters*, 43(23):012–12.
- Wiens, D. A. and Gilbert, H. J. (1996). Effect of slab temperature on deep-earthquake aftershock productivity and magnitude-frequency relations. *Nature*, 384:153–156.
- Wimpenny, S. and Watson, C. S. (2020). gWFM: A global catalog of moderate-magnitude earthquakes studied using teleseismic body waves. *Seismological Research Letters*, 92(1):212–226.

- Ye, L., Lay, T., and Kanamori, H. (2020). Anomalously low aftershock productivity of the 2019 MW 8.0 energetic intermediate-depth faulting beneath Peru. *Earth and Planetary Science Letters*, 549:116528.
- Zaliapin, I. and Ben-Zion, Y. (2013). Earthquake clusters in southern California I: Identification and stability. *Journal of Geophysical Research: Solid Earth*, 118(6):2847–2864.
- Zaliapin, I., Gabrielov, A., Keilis-Borok, V., and Wong, H. (2008). Clustering analysis of seismicity and aftershock identification. *Physical Review Letters*, 101(1):4–7.
- Zhan, Z. (2020). Mechanisms and Implications of Deep Earthquakes. *Annual Review of Earth and Planetary Sciences*, 48:147–174.
- Zhan, Z. and Shearer, P. M. (2015). Possible seasonality in large deep-focus earthquakes. *Geophysical Research Letters*, 42(18):7366–7373.

Figures

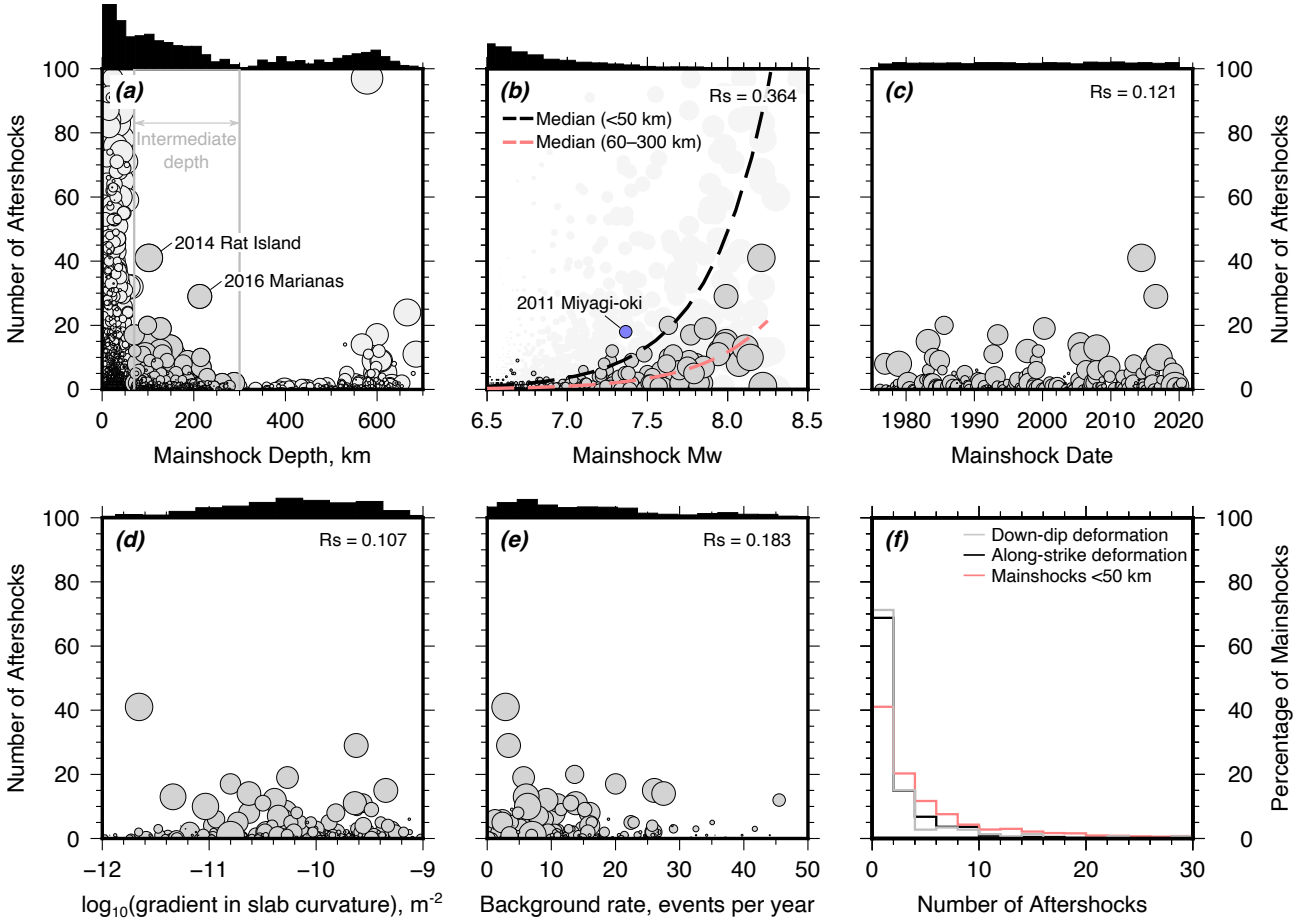


Figure 1: Aftershock productivity for earthquakes in the gCMT catalogue with $M_w \geq 6.5$. (a) Aftershock productivity as a function of the mainshock depth. Intermediate-depth earthquakes (60–300 km) are shown in dark grey. The histogram of the logarithm of mainshock frequency with depth is shown above. (b) Aftershock productivity as a function of mainshock magnitude. Intermediate-depth earthquakes are shown in dark grey with black outline, whilst earthquakes with hypocentral depths < 50 km (i.e. mainly those within the crust) are shown as light grey circles. The median productivity of the form $a10^{b(M-m_c)}$, where a and b are constants, M is the mainshock magnitude and $m_c = 4.5$, is shown for shallow (< 50 km) and intermediate-depth mainshocks in black and red, respectively. The Spearman’s Correlation Coefficient R_s for the intermediate-depth seismicity is shown in the top right. (c) Aftershock productivity as a function of mainshock date, (d) the gradient in the down-dip curvature of the slab at the centroid location computed from Slab 2.0 [Hayes et al., 2018], and (e) the background seismicity rate within 50 km horizontal distance and ± 30 km depth difference from the mainshock hypocentre. (f) Histogram of aftershock productivity for mainshocks that accommodate either along-strike or down-dip deformation of the slab. The red histogram shows the productivity for earthquakes with hypocentral depths < 50 km.

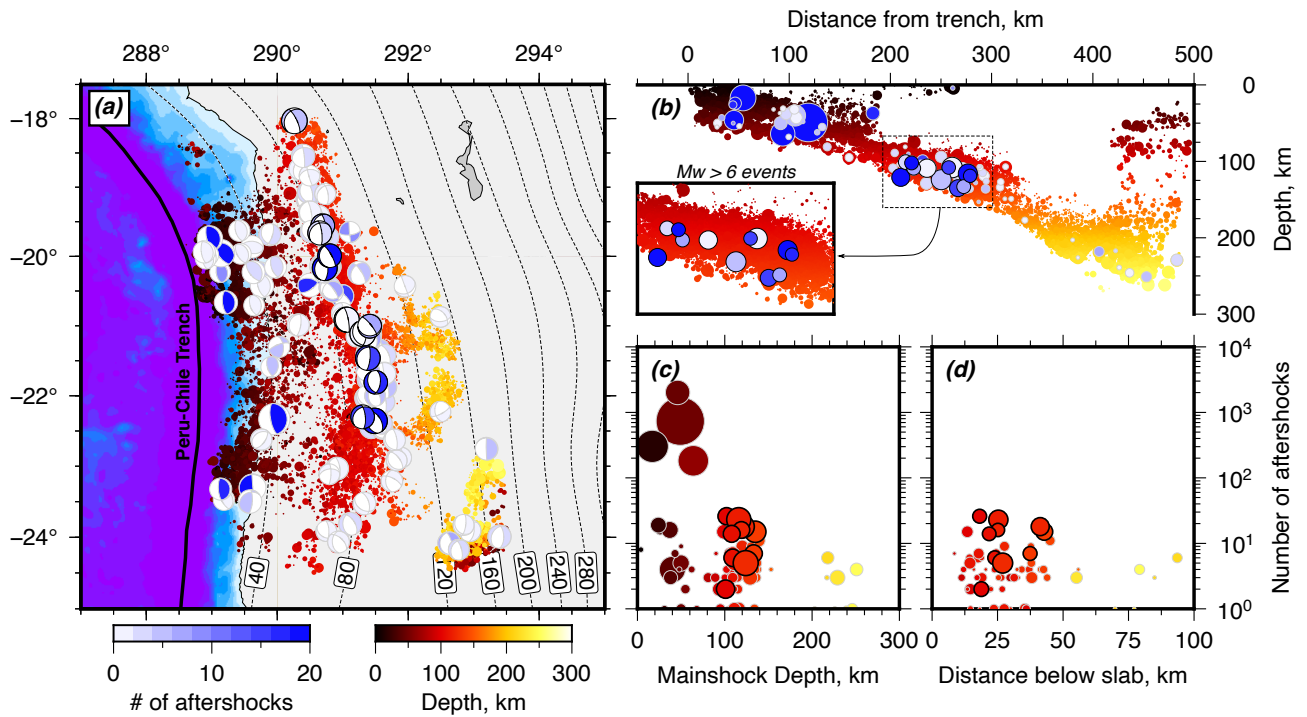


Figure 2: Aftershock productivity of moderate-magnitude earthquakes in northern Chile using the IPOC catalogue of Sippl et al. [2018]. (a) Map of the spatial distribution of the seismicity overlain with the focal mechanisms of the mainshocks taken from the gCMT catalogue. The focal mechanisms are coloured by the number of counted aftershocks. Mainshocks that are M_w 6.0–6.5 and at depths ≥ 70 km are highlighted by a black outline. Slab contours are from Slab 2.0 [Hayes et al., 2018]. (b) Cross-section through the IPOC seismicity overlain by the mainshocks shown as blue circles. Mainshocks are scaled by magnitude. (c) Aftershock productivity as a function of mainshock depth, and (d) depth below the slab surface. Only mainshocks with centroid depths > 70 km are plotted in (d).

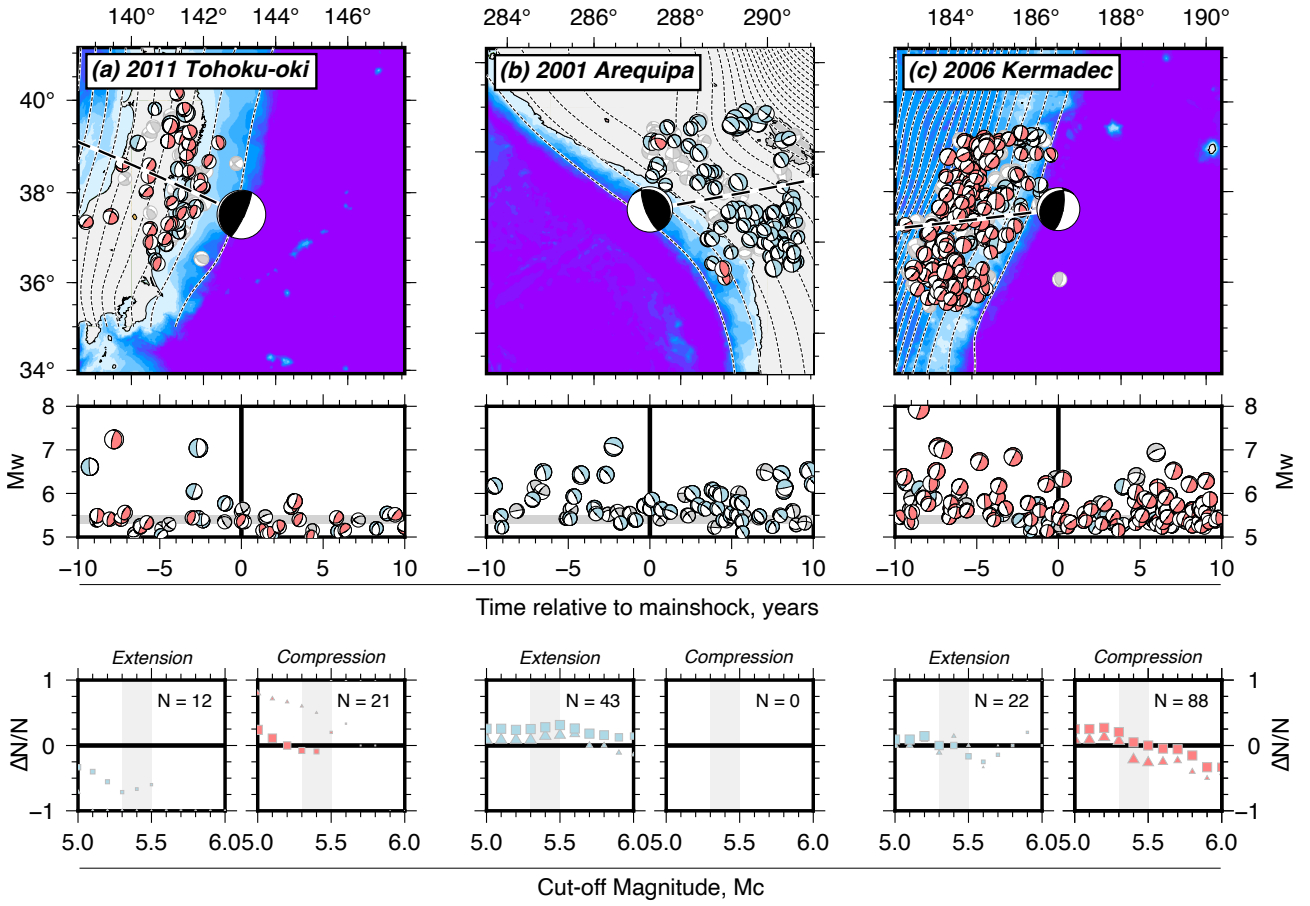


Figure 3: Examples of changes in intermediate-depth earthquake mechanisms before and after three major megathrust earthquakes. Mechanisms are coloured red if the are related to down-dip compression, blue for down-dip extension and grey for along-strike deformation. Contours represent the depth to the slab surface from Slab 2.0 [Hayes et al., 2018] and are every 20 km. The middle panel is a time-series of earthquake mechanisms as a function of magnitude. The dark grey horizontal line represents the global magnitude of completeness of the gCMT catalogue. The bottom panel shows the difference in the number of earthquakes after and before the megathrust event divided by the total number of earthquakes $\Delta N/N = (N_a - N_b)/(N_a + N_b)$, for down-dip extensional and compressional events. The vertical grey line shows the range of completeness for the gCMT catalogue. Squares and triangles represent $\Delta N/N$ for the period 5 years and 10 years either side of the mainshock, respectively. The size of the symbol is scaled by the number of earthquakes in that bin and decreases in size as the number of events in the bin gets smaller.

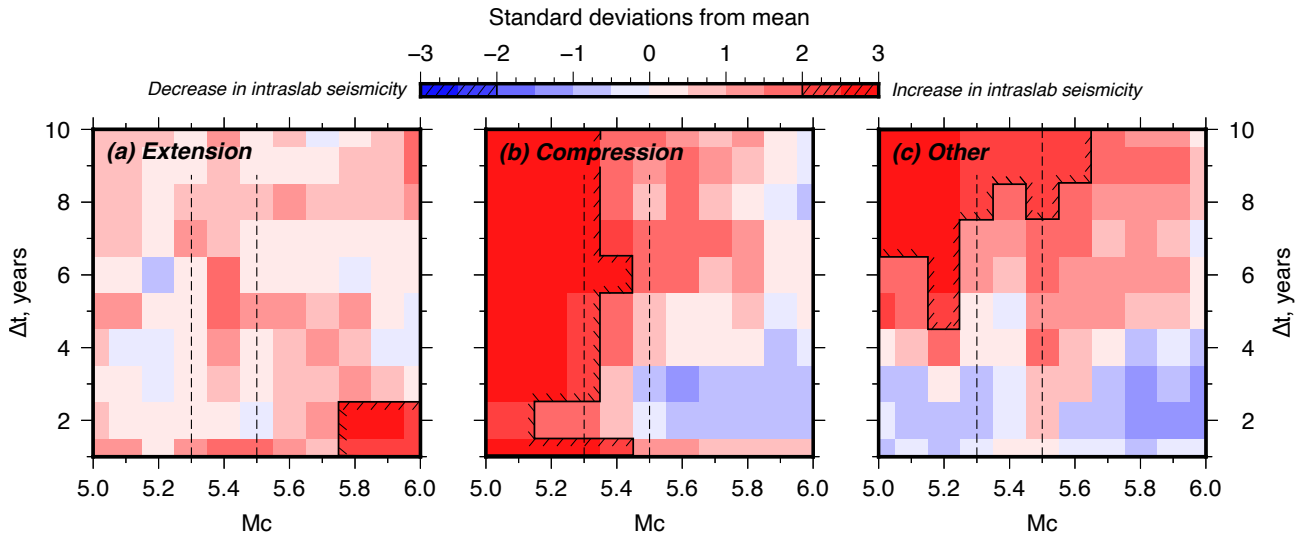


Figure 4: Compilation of changes in the frequency of intermediate-depth earthquakes following megathrust slip as a function of magnitude cut-off M_c and time-span Δt for (a) down-dip extensional, (b) down-dip compressional, and (c) other types of earthquakes. The colour in each panel represents the number of standard deviations from the mean distance that the summation reaches in k steps, equivalent to $\sum_{j=1}^k n_j / \sqrt{k}$. Given the null hypothesis is that an increase and a decrease in earthquake frequency are both equally likely, the expected value of $\sum_{j=1}^k n_j / \sqrt{k}$ is zero. The vertical dashed lines represent the approximate range in magnitude of completeness of the gCMT catalogue. The solid black line marks the 2 standard deviations boundary, with ticks on the inside of the boundary enclosing regions where the changes in earthquake frequency are unlikely to arise due to chance.

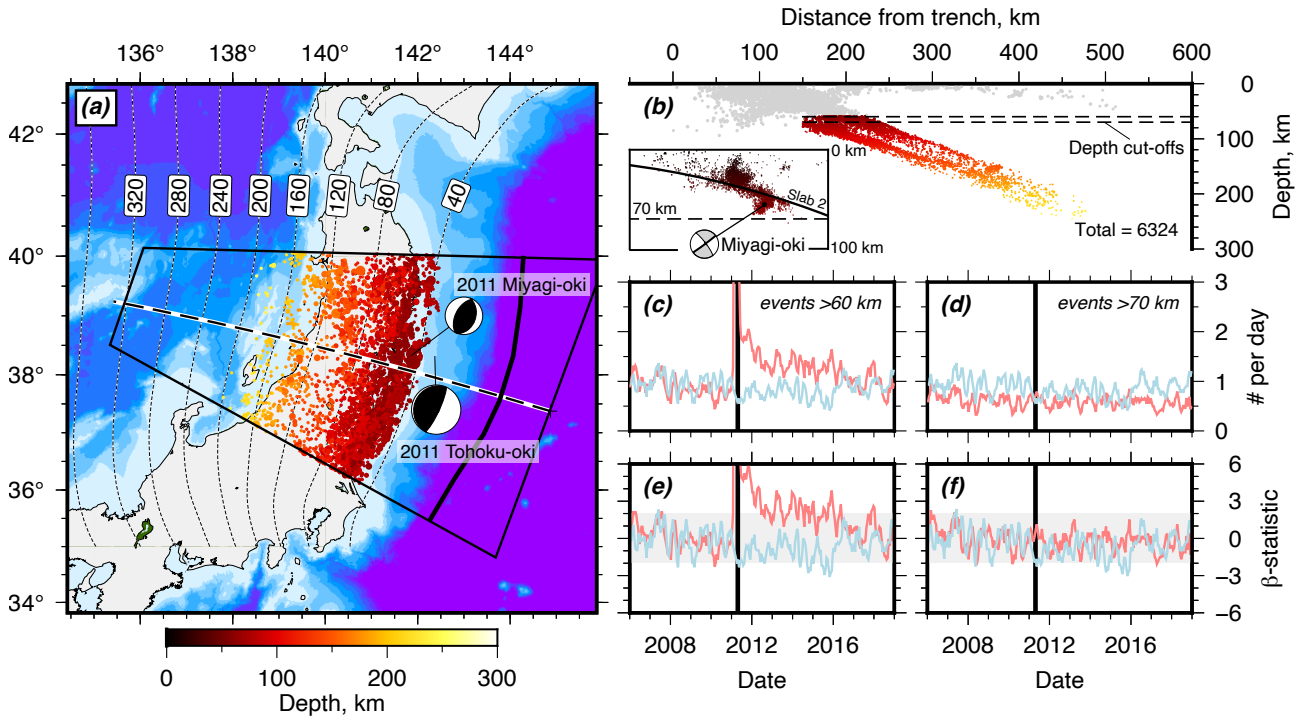


Figure 5: Temporal variations in intermediate-depth seismicity in response to the 2011 M_w 9.1 Tohoku-oki earthquake. (a) Spatial distribution of seismicity used in the analysis from the JMA catalogue. Contours of the slab surface are shown as black-dashed lines from Slab 2.0 [Hayes et al., 2018]. (b) Cross-section through the seismicity with the two depth cut-offs used in the analysis at 60 km and 70 km shown as black dashed lines. Inset is a zoom-in of the seismicity within ± 1 month of the 7th April 2011 Miyagi-oki earthquake with the 70 km depth cut-off shown. The aftershocks of the Miyagi-oki earthquake clearly extend 10–15 km below the slab surface, but remain shallower than 70 km depth. (c) Number of earthquakes per day in the upper plane (light red) and lower plane (light blue) of the double-seismic zone (DSZ) for all events >60 km depth. The time-series is calculated using a sliding window of length 0.2 years and time step 0.05 years. The vertical black line marks the timing of the Tohoku-oki mainshock. (d) Equivalent plot to (c), but for all events >70 km. (e) and (f) show the β -statistic of Matthews and Reasenberg [1988] for all events >60 km and >70 km depth, respectively. If β exceeds 2, this is equivalent to the earthquake rate deviating more than 2 standard deviations from background, with the background defined by the seismicity rate during the period 2006–2011.

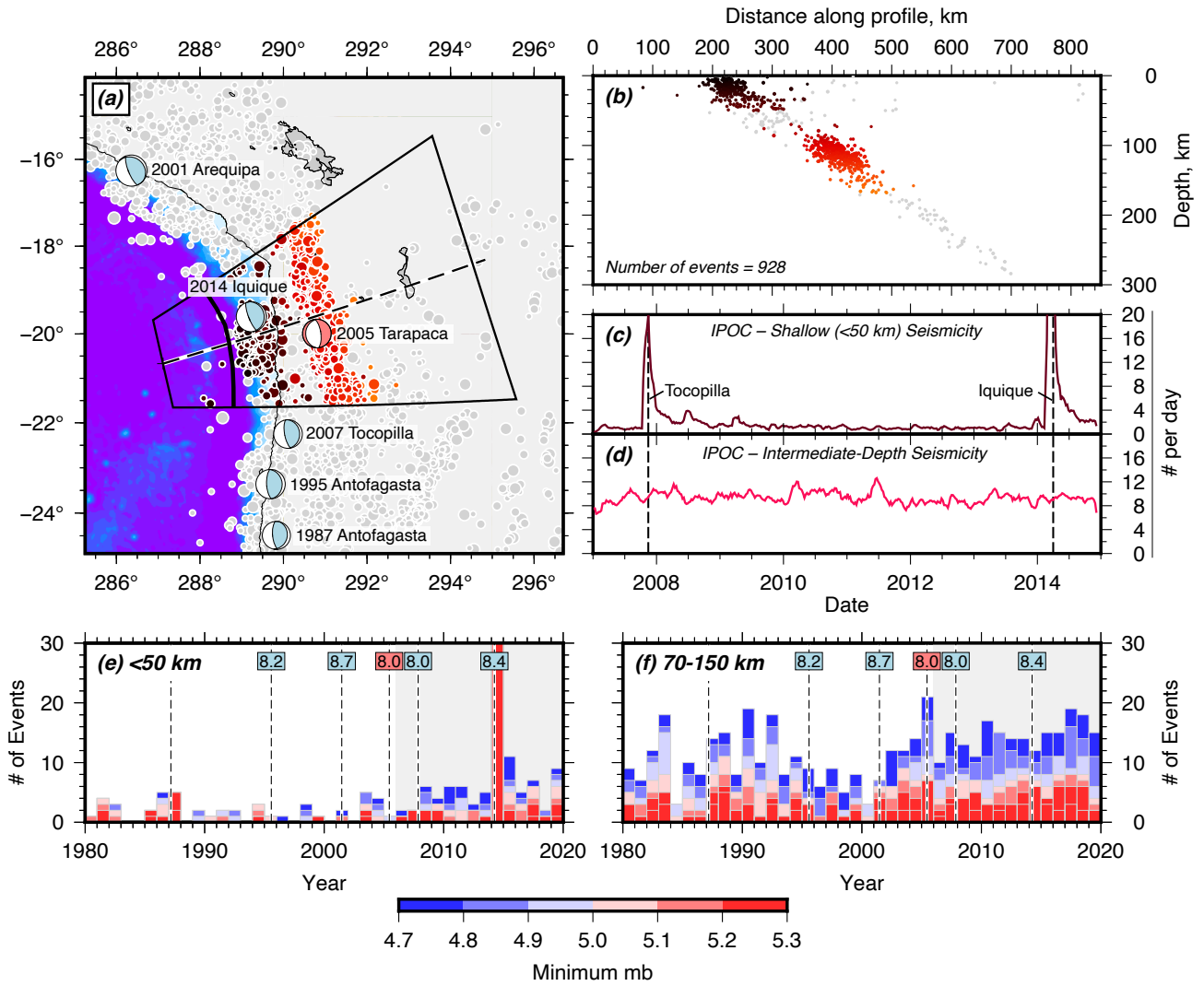


Figure 6: Overview of seismicity in northern Chile between 1980 and 2020. (a) Map view of the distribution of seismicity from the ISC catalogue with $m_b \geq 4.7$ and the mechanisms of the largest mainshocks. Grey circles represent earthquake hypocentres, and coloured circles represent earthquakes used in (b,e,f). (b) Cross-sectional view of the seismicity projected onto the black-dashed path in (a) showing the cluster of seismicity at ~ 400 km distance along the profile. (c) Temporal evolution of shallow (< 50 km) seismicity in northern Chile from the IPOC catalogue of Sippl et al. [2018] calculated using a sliding window of width 0.1 year and time steps of 0.02 years. (d) Same as (c), but for the intermediate-depth seismicity between 70 km and 300 km depth. (e) and (f) show histograms of the number of earthquakes in the ISC catalogue with $m_b > M$ each year for the shallow and intermediate-depth seismicity, respectively. The area in grey marks the installment of the IPOC network in northern Chile in 2006. Vertical dashed lines mark the timing of major earthquakes in the region and their magnitudes. Megathrust events are in light blue and intra-slab events are in light red.

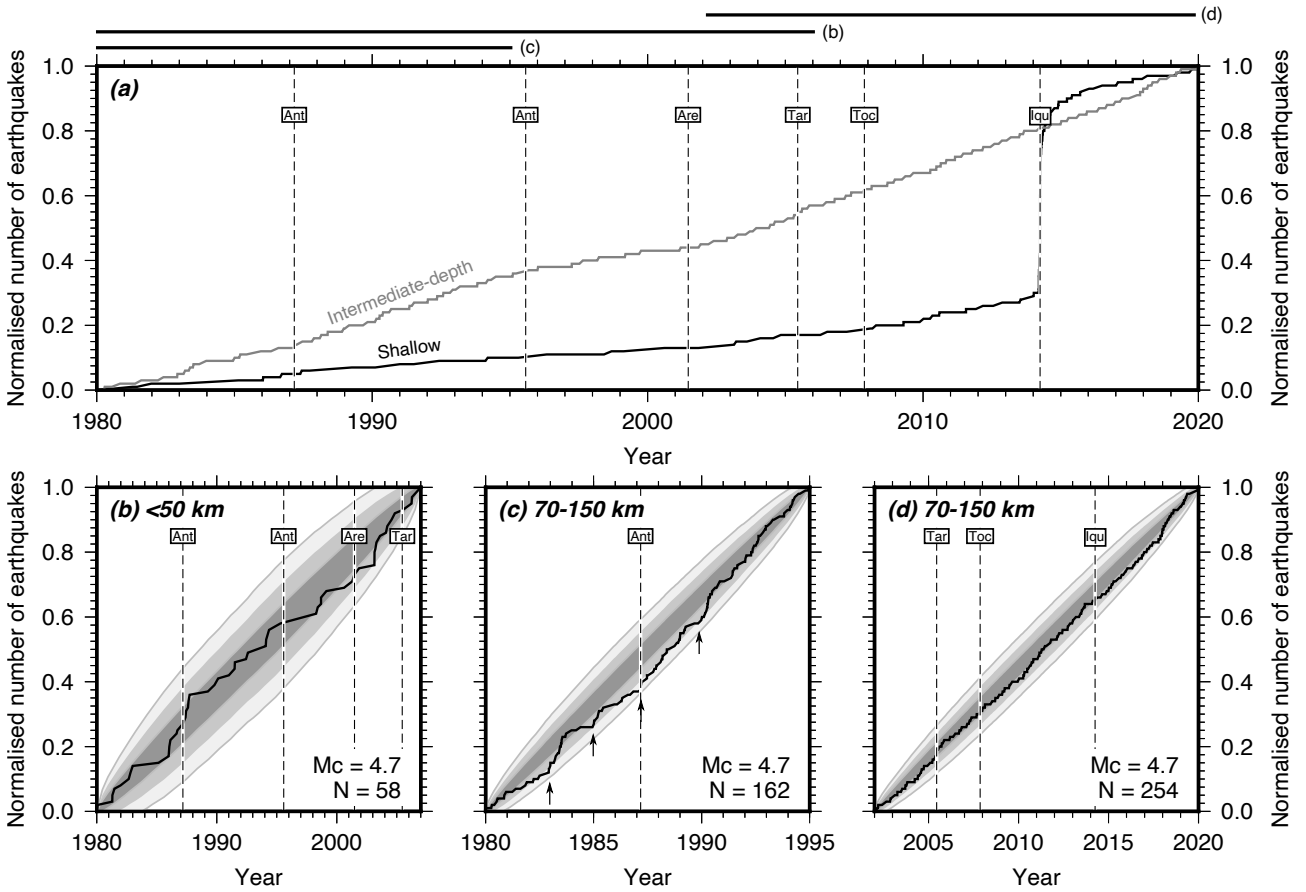


Figure 7: Cumulative distribution of shallow and intermediate-depth earthquakes in northern Chile shown in Figure 6a. (a) Cumulative distribution between 1980 and 2020 of events $m_b \geq 4.7$. Major ($M_w \geq 7.5$) megathrust and intermediate-depth earthquakes are shown by vertical dashed lines, with Ant = Antofagasta, Are = Arequipa, Tar = Tarapaca, Toc = Tocopilla and Iqu = Iquique. (b-d) Cumulative distributions of seismicity over particular periods of time compared to the predictions of time-randomised catalogues. The grey polygons show the area in which 67%, 95% and 99% of catalogues with the same number of events N but randomised earthquake times would plot. The confidence intervals are wider for catalogues with fewer events. In (c) vertical arrows point out distinct changes in the frequency of earthquakes that do not correlate with any major earthquakes. The equivalent plot for the declustered catalogue is shown in Supplementary Figure 6.

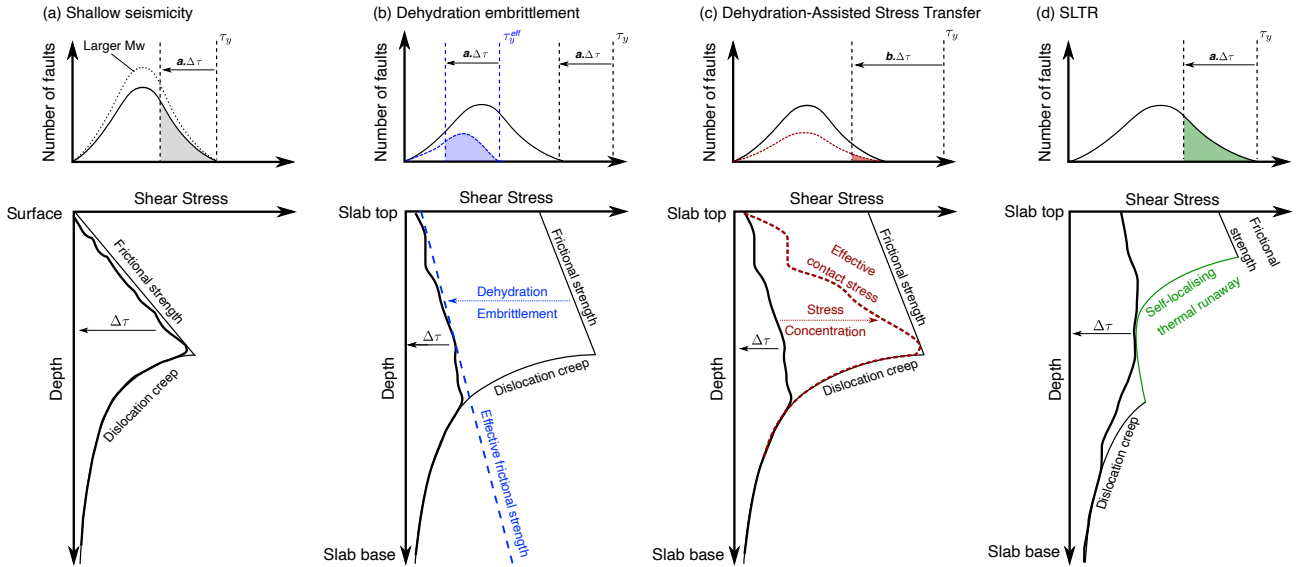


Figure 8: Sketch of the effect of stress transfer from an earthquake stress drop of amplitude $\Delta\tau$ on the triggering of nearby seismicity for (a) shallow earthquakes, and intermediate-depth earthquakes generated by (b) dehydration embrittlement, (c) dehydration-assisted stress transfer, and (d) self-localising thermal runaway (SLTR). For each mechanism, the top row shows the shear stress distribution on a population of seismogenic faults within a fixed (arbitrary) volume around the mainshock, where τ_y is the maximum failure stress for a given failure mechanism. In (b) and (c) the maximum failure stress would be dry olivine friction, or the effective failure stress τ_y^{eff} for faults containing highly-pressurised fluids. In (c) the maximum failure stress would be the stress needed to drive self-localising thermal runaway. The coloured region shows schematically the number of faults that would fail in aftershocks in response to a fixed stress transfer. The bottom row shows the failure strength envelope. The envelope shape in (d) is modified from John et al. [2009].